

Atomic force microscope nanolithography of graphene: Cuts, pseudocuts, and tip current measurements

R. K. Puddy,¹ P. H. Scard,¹ D. Tyndall,¹ M. R. Connolly,¹ C. G. Smith,¹ G. A. C. Jones,¹ A. Lombardo,² A. C. Ferrari,² and M. R. Buitelaar^{1,a)}

¹*Cavendish Laboratory, University of Cambridge, Cambridge CB3 0HE, United Kingdom*

²*Department of Engineering, University of Cambridge, Cambridge CB3 0FA, United Kingdom*

(Received 3 February 2011; accepted 7 March 2011; published online 1 April 2011)

We investigate atomic force microscope nanolithography of single and bilayer graphene. *In situ* tip current measurements show that cutting of graphene is not current driven. Using a combination of transport measurements and scanning electron microscopy we show that while indentations accompanied by tip current appear in the graphene lattice for a range of tip voltages, real cuts are characterized by a strong reduction in the tip current above a threshold voltage. The reliability and flexibility of the technique is demonstrated by the fabrication, measurement, modification, and remeasurement of graphene nanodevices with resolution down to 15 nm. © 2011 American Institute of Physics. [doi:10.1063/1.3573802]

Scanning probe microscopy, as well as being a powerful tool for imaging and spectroscopy, has also shown great potential for the manipulation and patterning of materials on the nanometer scale.^{1,2} Atomic force microscope (AFM) nanolithography, in particular, is now routinely used for the fabrication of quantum dots and quantum wires in materials such as Si and GaAs.^{3,4} AFM nanolithography also has significant potential for device fabrication in graphene, a material of intense current interest due to its exceptional mechanical, electronic, and optical properties.^{5,6} Most commonly, graphene nanoscale devices are fabricated using conventional electron-beam lithography and subsequent plasma etching.⁷⁻⁹ AFM lithography offers several advantages over electron-beam lithography: it has higher ultimate resolution, can be performed under ambient conditions and allows *in situ* device measurement and modification.

Usually AFM nanolithography is performed in air at room temperature. Under these conditions a water meniscus forms between the AFM tip and the substrate. The presence of an electric field, resulting from a voltage applied between the tip and substrate, dissociates water into hydrogen (H⁺) and hydroxyl (OH⁻) ions. When the voltage on the tip is negative with respect to the substrate the hydroxyl ions oxidize the graphene surface, creating the desired nanostructure. Several important factors determine the reliability and resolution of AFM lithography such as the applied tip voltage (or electric field strength), the humidity, tip velocity, applied force, and the conductivity of the substrate.¹ This process is now well understood for a variety of semiconductors and metals. However, in the case of graphene many of the key parameters have not been well established and device fabrication by AFM lithography is not yet routine. For example, the necessary threshold tip voltage for graphene oxidation reported in the literature varies in magnitude between ~-5 V (Ref. 10) and -35 V (Refs. 11 and 12) and in one report oxidation could only be initiated from a graphene edge.¹³ Moreover, there has been no systematic study of the tip current during AFM lithography of graphene.

Here, we investigate in detail the cutting of the graphene lattice with an AFM tip. In particular, we measure the tip current, I_{tip} , during the cutting process and find that we cut graphene only when I_{tip} drops below our noise floor. We also find that pseudocuts appear when I_{tip} is nonzero. These pseudocuts, in which the electron system of graphene remains intact, cannot reliably be distinguished from real cuts by AFM height imaging. However, the differences between real and pseudocuts become apparent using transport experiments and scanning electron microscopy (SEM). This ability to distinguish between real and pseudocuts is crucial for device fabrication in graphene.

To investigate the voltage and current dependence of AFM nanolithography on graphene we use a Veeco Dimensions 3100 AFM system with noncoated, doped silicon tips for both imaging and lithography.¹⁴ Imaging is performed in tapping mode and lithography carried out in contact mode. Single (SLG) and bilayer graphene (BLG) flakes are produced by micromechanical exfoliation on 300 nm SiO₂ with a highly doped Si back gate. Optical inspection and Raman spectroscopy¹⁵ are used to assess the layer number and quality. All flakes are electrically contacted and characterized at room temperature. Contacts are defined in polymethylmethacrylate (PMMA) resist by electron beam lithography and metalized with Ti/Au (5/50 nm) by evaporation and lift off.

Samples are annealed for ~10 min at 300 °C in forming gas prior to AFM lithography, which we find to be a crucial step for reliable cutting of our flakes as it removes contamination such as PMMA residues which can prevent oxidation. During AFM nanolithography, we use a 50 nm/s scanning speed and a relative humidity of around 50%. The lithographically defined trenches vary in width from 15 nm up to 100 nm with typical values of 30 nm. We find that the widths depend only weakly on scanning speed and humidity, with cuts slightly wider with decreasing scanning speed and increasing relative humidity. Individual tip characteristics, most likely tip radius, appear to be more important.

We first investigate the current through the biased AFM tip during lithography. Figure 1 shows a series of cuts performed on a SLG at various tip voltages. The AFM tip is

^{a)}Electronic mail: mrb51@cam.ac.uk.

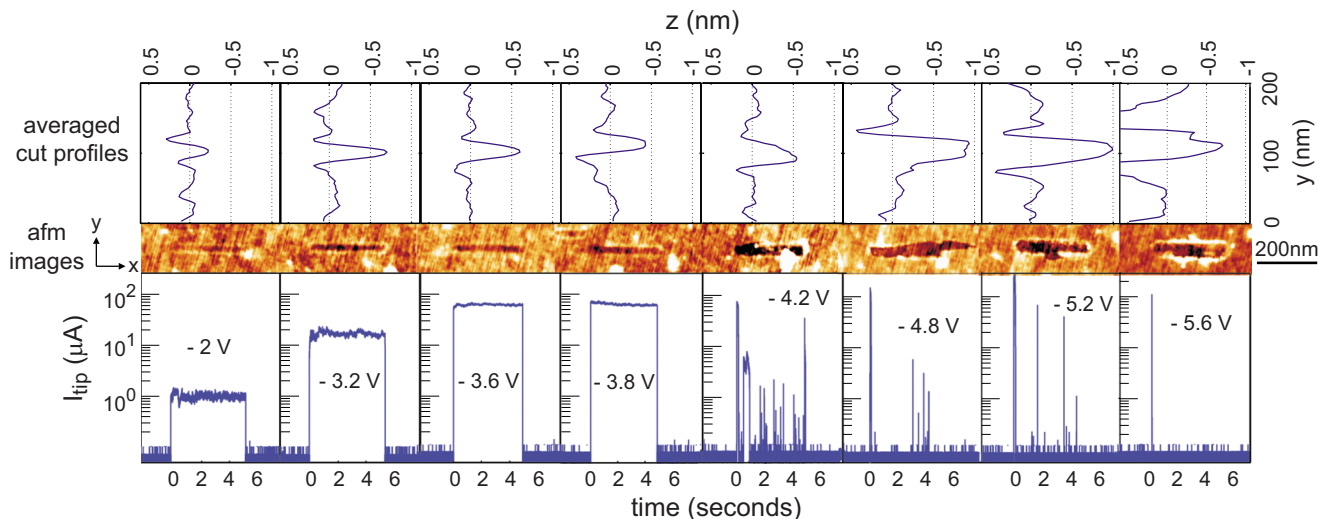


FIG. 1. (Color online) A series of cuts or indentations in a SLG flake, made using an AFM tip in contact mode at increasingly negative voltages relative to the grounded flake. The upper panels show the averaged height profile cross-sections of the cuts, the central panels show the corresponding AFM micrographs and the bottom panels show the current, I_{tip} , through the AFM tip as a function of time t , recorded during the cutting process where $t=0$ is the start of tip contact. The series is performed using a single, non coated, doped silicon tip (Ref. 14). Tip speed was 50 nm/s and the relative humidity was $\sim 50\%$.

negatively biased with respect to the flake, which is grounded via a Stanford SR570 current preamplifier. The lower panels of Fig. 1 show the current, I_{tip} , through the tip to ground, as a function of time where $t=0$ is the time at which the tip bias V_{tip} is applied and the tip starts along its predefined path. Above this is the corresponding AFM image of the scanned area. The upper cells show the averaged height cross section across the cuts. Indentations begin to appear on the graphene surface, accompanied by finite I_{tip} , at around $V_{tip} = -2$ V. The tip current then drops to ~ 0 above a threshold, V_{thresh} . Threshold voltages for our tips vary from ~ -3.5 V to ~ -5 V. Trenches created at the smallest voltages occasionally disappear over the course of hours or days, regaining their original shape. Trenches created at larger voltages remain unchanged after several weeks. We also note that, in both regimes, ridges are frequently formed along the trench edges where the electric field is lower. This may be due to the formation of stable oxides similar to that reported in Refs. 10 and 11.

To investigate the nature of the marks created in the two regimes we cut triangles into a SLG with V_{tip} both above and below V_{thresh} and imaged them using both AFM and SEM. Figures 2(a) and 2(b) show two triangles, cut with $|V_{tip}| > |V_{thresh}|$ and thus $I_{tip} \sim 0$, imaged using AFM (left image) and SEM (right image). The central regions of the triangles, clearly visible in the AFM image, are significantly darker in the SEM images as compared to the bulk. Figures 2(c) and 2(d) show two triangles, cut with $|V_{tip}| < |V_{thresh}|$ and $I_{tip} \sim 100 \mu\text{A}$, again imaged using AFM (left) and SEM (right). Though the AFM images are qualitatively similar to those in Figs. 2(a) and 2(b), the triangles are barely visible in the SEM images with the central regions showing no contrast with the bulk. In all cases, SEM imaging is carried out using an accelerating voltage of 500 V. Note that for these low acceleration voltages (i.e., below ~ 1 kV), the contacted graphene is easily visible on the SiO_2 substrate. This is illustrated in Figs. 2(e) and 2(f) which show SEM images of the areas of the flake on which the triangles were cut. The arrows indicate the locations of the triangles in Figs. 2(a)–2(d). The strong contrast of the graphene flakes on the SiO_2 substrate is

attributed to differences in the surface electrostatic potential between the bare SiO_2 substrate and the regions covered by the (electrically contacted) graphene, similar to that observed for carbon nanotubes.¹⁶ This immediately allows us to conclude that the triangles shown in Figs. 2(a) and 2(b), which appear dark in the SEM images, are electrically isolating, while those of Figs. 2(c) and 2(d) are electrically connected to the bulk. This behavior is consistent over all ten pairs of triangles measured.

For further confirmation, the tip is placed inside the triangles and voltages below threshold are applied. We find that

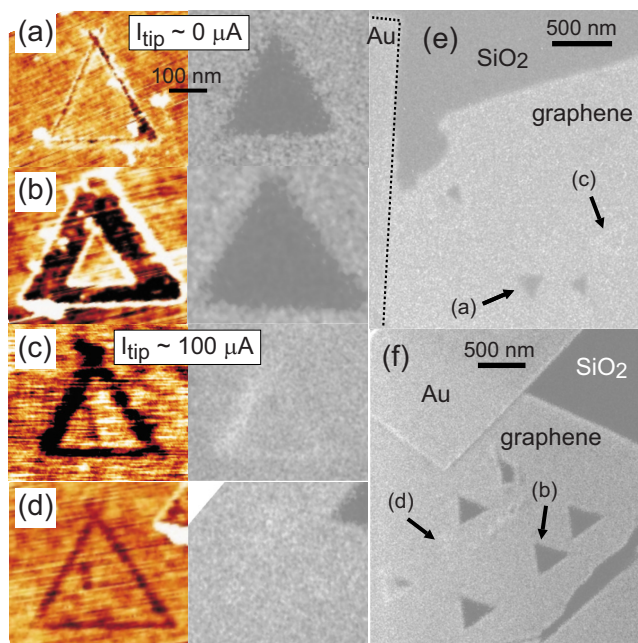


FIG. 2. (Color online) [(a) and (b)] AFM (left) and SEM images (right) of two triangles cut with $|V_{tip}| > |V_{thresh}|$ such that the tip current, $I_{tip} \sim 0$ during cutting. [(c) and (d)] AFM (left) and SEM images (right) of two triangles cut with $|V_{tip}| < |V_{thresh}|$ such that $I_{tip} \sim 100 \mu\text{A}$ during cutting. [(e) and (f)] SEM images of the areas of the graphene flake on which the triangles were cut. The arrows indicate the locations of the triangles shown in panels [(a)–(d)].

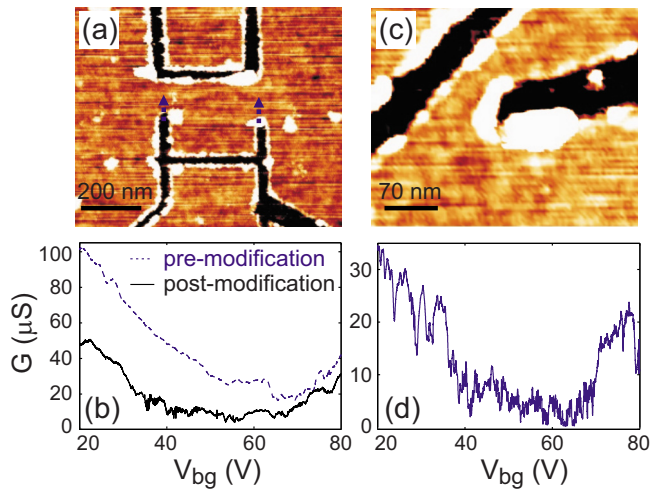


FIG. 3. (Color online) (a) AFM image of a quantum dot formed in BLG using AFM nanolithography. The entrances are initially ~ 150 nm. In a second AFM lithography step these are narrowed to ~ 50 nm, as indicated by the arrows (b) Conductance vs V_{bg} at $T=4.2$ K of the quantum dot pre (dashed curve) and postmodification (solid curve). (c) AFM image of a ~ 65 nm constriction formed in a bilayer flake (d) Conductance vs V_{bg} for the constriction measured at $T=4.2$ K.

we never measure current above our noise floor with triangles cut with $|V_{tip}| > |V_{thresh}|$ while we always measure current with triangles cut with $|V_{tip}| < |V_{thresh}|$. Furthermore, the current measured from within these triangles is no smaller than the current measured from outside the triangles. The resulting indentations can be seen as the short lines within Figs. 2(c) and 2(d) whereas no such marks are seen in Figs. 2(a) and 2(b). We conclude that electrically isolating cuts are made only for negative tip voltages larger than $|V_{thresh}|$ at which point the applied electric field is sufficiently strong to initiate the oxidation process. As graphene is oxidized below the tip, the tip-graphene contact is disrupted and I_{tip} vanishes.¹⁷ We believe that for tip voltages below the threshold, the SLG is merely pressed into contact with the SiO_2 surface by displacing water trapped between graphene and the substrate. The graphene in this case remains unbroken and electrically conducting.

Finally, we show that the technique described is well suited for device fabrication. Figures 3(a) and 3(c) show AFM images of two graphene nanodevices, designed as quantum dot and quantum wire, respectively, formed in a BLG by AFM nanolithography. For each device, the tip current is monitored during lithography to ensure that the graphene is properly cut. Figures 3(b) and 3(d) show the conductance as a function of back gate voltage V_{bg} of the devices at a temperature of 4.2 K. The flexibility of AFM lithography is illustrated by Fig. 3(b) which shows measurements of the conductance as a function of V_{bg} at 4.2 K both for the quantum dot as shown in Fig. 3(a) (dashed line) as

well as that of the same device but with the entrance barriers of the quantum dot narrowed from ~ 150 nm to about 50 nm in a subsequent AFM lithography step at room temperature (solid line). As expected, the conductance is significantly lower in the post modification device with an increase in the gap observed.⁷

In conclusion, we have studied the local oxidation of graphene by an AFM tip. We demonstrate that at low tip voltages the graphene is typically not cut even though clear indentations are observed in AFM height images. The lattice is only cut when the local electric field exceeds a threshold at which point tip current vanishes (within our noise floor). These conclusions are supported by SEM and transport experiments. The ability to distinguish between pseudocuts and cuts as demonstrated here is important for reliable graphene device fabrication by AFM nanolithography.

We acknowledge Cinzia Casiraghi for technical support. A.C.F. and A.L. acknowledge funding from EU grants NANOPOTS and RODIN, EPSRC Grant No. EP/G042357/1 and a Royal Society Wolfson Research Merit Award. M.R.B. acknowledges support from the Royal Society.

- ¹A. A. Tseng, A. Notargiacomo, and T. P. Chen, *J. Vac. Sci. Technol. B* **23**, 877 (2005).
- ²L. Tapasztó, G. Dobrik, P. Lambin, and L. P. Biró, *Nat. Nanotechnol.* **3**, 397 (2008).
- ³P. M. Campbell, E. S. Snow, and P. J. McMarr, *Appl. Phys. Lett.* **66**, 1388 (1995).
- ⁴U. F. Keyser, H. W. Schumacher, U. Zeitler, R. J. Haug, and K. Eberl, *Appl. Phys. Lett.* **76**, 457 (2000).
- ⁵A. K. Geim and K. S. Novoselov, *Nature Mater.* **6**, 183 (2007).
- ⁶F. Bonaccorso, Z. Sun, T. Hasan, and A. C. Ferrari, *Nat. Photonics* **4**, 611 (2010).
- ⁷M. Y. Han, B. Özyilmaz, Y. B. Zhang, and P. Kim, *Phys. Rev. Lett.* **98**, 206805 (2007).
- ⁸L. A. Ponomarenko, F. Schedin, M. I. Katsnelson, R. Yang, E. H. Hill, K. S. Novoselov, and A. K. Geim, *Science* **320**, 356 (2008).
- ⁹C. Stampfer, E. Schurtenberger, F. Molitor, J. Güttinger, T. Ihn, and K. Ensslin, *Nano Lett.* **8**, 2378 (2008).
- ¹⁰S. Neubeck, L. A. Ponomarenko, F. Freitag, A. J. M. Giesbers, U. Zeitler, S. V. Morozov, P. Blake, A. K. Geim, and K. S. Novoselov, *Small* **6**, 1469 (2010).
- ¹¹L. Weng, L. Zhang, Y. P. Chen, and L. P. Rokhinson, *Appl. Phys. Lett.* **93**, 093107 (2008).
- ¹²S. Masubuchi, M. Ono, K. Yoshida, and T. Machida, *Appl. Phys. Lett.* **94**, 082107 (2009).
- ¹³A. J. M. Giesbers, U. Zeitler, S. Neubeck, F. Freitag, K. S. Novoselov, A. K. Geim, and J. C. Maan, *Solid State Commun.* **147**, 366 (2008).
- ¹⁴The AFM tips are highly doped Si tips with a force constant of 42 N/m. Estimated forces during lithography are in the 1–10 μN range.
- ¹⁵A. C. Ferrari, J. C. Meyer, V. Scardaci, C. Casiraghi, M. Lazzeri, F. Mauri, S. Piscanec, D. Jiang, K. S. Novoselov, S. Roth, and A. K. Geim, *Phys. Rev. Lett.* **97**, 187401 (2006).
- ¹⁶T. Brintlinger, Y.-F. Chen, T. Dürkop, E. Cobas, M. S. Fuhrer, J. D. Barry, and J. Melngailis, *Appl. Phys. Lett.* **81**, 2454 (2002).
- ¹⁷The expected electron flow of the oxidation reaction is small and below our measurement resolution. Additional measurements (not shown) indicate that during AFM lithography $I_{tip} < 1$ nA.